Segregation Phenomena in Thin Films of Strongly Asymmetric Diblock Copolymers Deposited onto Solid Substrates

V. W. Stone,[†,§] C. Poleunis,[‡] P. Bertrand,[‡] R. Legras,[†] and A. M. Jonas*[,†]

Unité de Chimie et de Physique des Hauts Polymères and
Unité de Physique et de Physico-Chimie des Matériaux, Université catholique de Louvain,
1 Place Croix du Sud, B-1348 Louvain-la-Neuve, Belgium

Received March 10, 1999; Revised Manuscript Received February 18, 2000

ABSTRACT: Thin films (300 Å) of homodisperse polystyrene (PS) chains tagged at one end by a short chlorinated polybutadiene (CPB) segment have been spin-coated on Si wafers covered or not by a thin (300 Å) layer of amorphous carbon. These strongly asymmetric P(CB-*b*-S) diblock copolymers do not microphase-separate in the bulk. Depth profiles from X-ray reflectivity (XRR) and DSIMS have been obtained on thin films of this diblock before and after annealing. Whatever the surface studied, the electron density profiles derived from XRR measurements did not show any significant difference with the ones obtained with homodisperse PS. By contrast, DSIMS and XPS experiments showed a clear depletion of the CPB short block starting from the air interface when the copolymers are deposited onto the silicon substrates. Such a depletion cannot be detected when the copolymers are deposited onto the almost apolar carbon surface. This suggests a preferential accumulation of the chlorinated block toward the silicon oxide polar surface, in agreement with an estimation of the interfacial energy reduction implied by the process, indicating that segregation effects in these systems are dominated by energetic balances.

Introduction

The behavior of symmetric diblock copolymers in thin films and near interfaces has been extensively studied over the past 10 years, both below and above the bulk order−disorder transition temperature (ODT).[1−11] It has been invariably shown that one of the blocks preferentially segregates to the solid interface, due to its lower interfacial energy. Above the bulk ODT, this results in a damped periodic lamellar-like fluctuation of composition starting from the solid interface, which implies that no true order−disorder transition temperature can be defined for thin films of symmetric diblocks.[7]

By contrast, much less work has been performed on the ordering of asymmetric diblock copolymers near solid or gaseous interfaces. Most works in this field have focused on the packing of spherical or cylindrical micelles near interfaces for copolymers well below their ODT.[12−18] Aside from specific orientation and ordering of mesophases with respect to the interfaces, preferential segregation of one block to the interfaces was also observed in many circumstances, with the formation of a lamellar-like arrangement sometimes being detected at the immediate vicinity of the interfaces.[14,16,18] To our knowledge, there has been so far no work on the behavior of strongly asymmetric diblock copolymers near interfaces at temperatures above their ODT. For sake of completion, we mention that recent segregation studies on blends of a homopolymer and a strongly asymmetric fluorine-containing diblock,[19] and on multiblock copolymers with a small volume content of fluorinated blocks,[20] have shown interface segregation phenomena to occur as well for such systems.

Provided their molecular mass is not too large, strongly asymmetric diblock copolymers resemble somewhat systems that have been more extensively studied, i.e., polymer chains tagged at one end in order to study chain end segregation phenomena. Far from being exclusively of academic interest, the determination and control of polymer chain-end distribution at interfaces are of crucial importance in many practical applications. Good examples are crack healing in elastomeric materials[21] and particle coalescence in latex films formation.[22] Within the chain reptation picture, the rate of these processes critically depends on the initial end distribution at the surface. Moreover, functional termini onto chains can dramatically change the surface and interfacial properties of polymer materials. Because of the multiplicity and complexity of the factors responsible for chain-end segregation phenomena, comprehensive studies performed on well-defined systems were recently performed.

Chain-end segments almost always differ chemically from each other and from the chain segments, due to the way the polymer was synthesized (e.g., initiating and terminating agents generally introduce specific groups at the ends of anionically synthesized polymers) and/or to the intentional introduction of labels near the ends in order to facilitate their detection. In this context, if end segments are in sufficient number with surface energies sufficiently different from the chain segments, then they may segregate by interfacial energy reduction. Interfacial energy reduction is the overwhelming factor controlling chain end segregation, while entropic effects which were theoretically predicted[23−26] are usually undetectable due to their weakness.

Most previous studies used deuterium labeling to localize chain ends in thin homodisperse polystyrene films deposited onto silicon wafers, using secondary ion mass spectrometry in static (SSIMS)[27] or in dynamic mode (DSIMS)[28] and neutron reflectometry (NR).[28−30] Even for polymers that had not been intentionally functionalized, these studies have highlighted the very subtle balance which exists between the various factors

[†] Unité de Chimie et de Physique des Hauts Polymères.
[‡] Unité de Physique et de Physico-Chimie des Matériaux.
[§] Current address: UCB Chemicals s.a., Research and Technology, 33 rue d'Anderlecht, B-1620 Drogenbos, Belgium.

10.1021/ma990364f CCC: $19.00 © 2000 American Chemical Society
Published on Web 05/19/2000

controlling segregation at interfaces. Studies carried out on polystyrenes (PS) tagged at one end have shown that segregation toward interfaces is the result of a competition between the initiator fragment at one end and the deuterated labeling segment at the other end. The former which is most often a short hydrocarbon segment (such as a *sec*-butyl group) has a surface energy lower than that of PS[30] and will thus tend to drive its connected segments to free surfaces. The latter may segregate to both neutral interfaces and polar substrates (e.g., silicon oxide)[31] for which deuterium species are known to have higher affinity than hydrogen segments.[31] Neglecting in first approximation the spatial constraints imposed on segments in block copolymers, this behavior may be rationalized by the use of energetic arguments, similarly to recent experimental[31] and theoretical studies[32] on segregation phenomena in binary phase mixed blends of polymers symmetric in molecular weight. For blends far from their bulk critical point, segregation toward interface i is mainly driven by the net difference in adsorption energies between segments of polymer 1 and 2:

$$\chi_i = \frac{\left[(\epsilon_{1i} - \epsilon_{2i}) - \frac{1}{2}(\epsilon_{11} - \epsilon_{22})\right]}{kT} \qquad (1)$$

where ϵ_{1i} (ϵ_{2i}) represents the interaction energy of polymer segments 1 (2) with an attractive ($\epsilon > 0$) or repulsive ($\epsilon < 0$) interface, and $\epsilon_{11} > 0$ ($\epsilon_{22} > 0$) is the net interaction energy experienced by two segments of polymer 1 (2) in the bulk. Even if the interface is neutral ($\epsilon_{1i} = \epsilon_{2i} = 0$), a net difference in surface energies exists because species at the interface feel a loss of potential energy by the lack of neighbors at the interface compared to the bulk.[33] The system thus tends to partition to the interface the segments having the weakest pair interaction in the bulk. A positive (negative) χ_i therefore means segregation of 1 (2) species to interface. In particular, deuterated segments tend to segregate to neutral interfaces in isotopic polystyrene blends ("isotopic effect").[34] Identifying component 1 to deuterated styrenes (D) and 2 to hydrogenous styrenes leads to $\chi_i > 0$ as $\epsilon_{HH} > \epsilon_{DD}$.[35] A fortiori, when i is polar, $\epsilon_{Di} > \epsilon_{Hi}$[31] and then $\chi_i \gg 0$, meaning that the segregation of deuterated segments is reinforced.

The purpose of this paper is to evaluate the interplay of the above-mentioned factors in systems where, instead of deuterated polystyrene, a short chlorinated polybutadiene segment is used as label. Because of the variety of phenomena already evidenced in the deuterated systems, a system having a simple polymer architecture was selected: homodisperse polystyrene chains having at one end a hydrogen atom and at the other a short chlorinated polybutadiene block terminated by a *sec*-butyl group. Our system is actually closer to a strongly asymmetric diblock copolymer than to an end-tagged homopolymer. Chlorine atoms were introduced in order to discriminate one of the chain ends from the other segments by X-ray reflectometry (XRR), DSIMS, or X-ray photoelectron spectroscopy (XPS). With this system, energy-driven segregation phenomena, if any, should result: (a) from differences in interactions energies between chlorinated segments and between styrene segments; (b) from differences in the affinity of chlorinated and styrene segments for nonneutral surfaces. Despite the incompatibility existing between chlorinated polybutadiene and polystyrene at 150 °C,[36] the copolymer chains are much too short and asymmetric in block length to phase segregate.[37] The strongly asymmetric diblocks were deposited onto surfaces having different surface energies in order to assess the influence of the adsorptive properties of the substrate (silicon with its native oxide layer, amorphous carbon).

Experimental Section

Characterization Techniques. X-ray reflectivities were measured with a θ/θ goniometer whose geometry is described elsewhere.[36] Data were corrected for spillover effects.[36] Electron density profiles were obtained from the data using procedures extensively described elsewhere.[36] Basically, these profiles were first approximated by a succession of M slabs of uniform density ρ_i ($1 \le i \le M$, $i = 0$ is the substrate). From this model, the reflectivity can be computed by Parrat's method;[38] the thickness and density of each slab were then optimized in order to minimize

$$\chi^2 = \sum_{j=1}^{N}\left(\frac{R_{\mathrm{meas},j} - R_{\mathrm{calc},j}}{w_j}\right)^2 + \lambda\sum_{i=0}^{M-1}(\rho_{i+1} - \rho_i)^2 \qquad (2)$$

In eq 2, the first term is a weighted sum of residuals obtained from the N measured reflectivities $R_{\mathrm{meas},j}$ and corresponding reflectivities calculated from the model density profile, while the second term is a regularizing term introduced to avoid spurious oscillations in the electron density profiles.[39] The standard error on each point j was taken as weight (w_j), except in the first stages of the fit where empirically determined weights were used to favor convergence.[36] The whole fitting process was repeated with increasing number of slabs (M) until each slab was sufficiently thin not to introduce artificial oscillations in the computed reflectivity over the experimental angular range.[40] From this discrete profile, a continuous profile was computed, consisting in a superposition of 2−3 virtual layers each with its own thickness, density, and roughness. The final fit was performed with this simplified model. Calculated reflectivities were convolved by a Gaussian resolution function estimated from the divergence of the beam and the wavelength distribution.[36] Dark noise, surface diffuse scattering, and scattering from the bulk sample were taken into account by the use of a constant background whose value was determined from the intensity either side of the specular peak.

Dynamic secondary ion mass spectroscopy profiles were obtained with a Riber-Q156 SIMS spectrometer which consists of a 45° deflection energy selector and a quadrupole mass filter. The detection of secondary ions was done at 90° with respect to the ion beam direction. DSIMS profiles were performed under ultrahigh vacuum (10^{-9} Torr) using a hot cathode ion source (Kratos WG-535); during etching, the noble gas pressure rises to about 3×10^{-7} Torr. Typical working conditions for ion beam sputter etching and SIMS analysis were as follows: a 200 μm diameter Xe^+ (4 keV) ion beam is rastered over a 1.7×0.7 mm^2 area with mean target currents varying between 10.2 and 13.4 nA. Current variations never exceeded 1 nA during profiles acquisition. The incidence angle with respect to the normal of the sample surface was 45°. An electronic gate was used so that the SIMS signal only came from the central part of the crater (9% of the total bombarded surface). Automatic sequences of analysis and sputter depth profiling were programmed with a multichannel analyzer (Ortec) and treated using homemade software. Concentration depth profiles were obtained by storing successively as a function of bombardment time the SIMS intensities of C^-, O^-, Si^-, and Cl^- accumulated during respectively 5, 5, 10, and 10 s. Polymers being insulators become charged when ion bombarded. This effect was canceled by use of an electron flood gun (VSW-EG2) sending low-energy electrons (200 eV) onto the sample during the measurements. Uncontrolled ion beam displacement during analysis and sputter depth profiling was thus reduced to a minimum. As we were only interested in a

qualitative analysis of the profiles formed, no depth scale calibration or deconvolution of the SIMS data were carried out.

X-ray photoelectron spectroscopy (XPS) measurements were performed with a SSI X-probe (SSX-100 model 206) photoelectron spectrometer from Surface Science Instruments (Fisons, U.K.), using a monochromatized aluminum anode (10 kV, 20 mA). The spectrometer was interfaced with a Hewlett-Packard 9000/310 computer and operated in the fixed analyzer transmission (FAT) mode. Large sample areas (elliptic spots with shorter axis of 1000 μm) were rastered in order to minimize collection time and hence possible radiation damage to the polymers. A survey scan (0−1100 eV) was recorded for each sample, followed by high-resolution scans of C(1s), O(1s), Si-(1s), Si(2s), Cl(2s), and Cl(2p) peaks where appropriate; this run was ended by a C(1s) check for eventual sample degradation. Survey scans were performed by setting the analyzer energy to 150 eV and using low acquisition times. Longer accumulation times with an analyzer energy set to 50 eV were used for the high-resolution scans. To minimize sample charging, an electron flood gun set at 6 eV and 55 μA[41] was used with a nickel grid placed 3 mm above the sample surface. No charge compensation was needed for the carbonaceous samples. Binding energies were referenced to the C(1s) of the C(−C,H) peak, set at 284.8 eV. The pressure in the analyzing chamber was around 10^{-9} Torr. All experiments were run at room temperature. Elemental surface compositions were expressed in at. %, neglecting the H content not detected by XPS, and computed from relative areas under peaks and elemental sensitivity factors provided by the SSI instrument software. Before performing this analysis, survey and high-resolution spectra had been normalized for constant acquisition times. A linear background was subtracted from the peaks.

Substrate Preparation. To evaluate the influence of the polymer segment/substrate surface energetics in segregation phenomena, substrate surfaces of different surface energies were prepared. Because of the constraints imposed by XRR, all substrates must be sufficiently smooth and flat over areas larger than 1 cm^2. The 1.5 × 1.5 cm^2 samples were cut from 2 in. diameter silicon wafers (n-type, ⟨100⟩ orientation, Wäcker). Immediately prior use, all silicon pieces were cleaned in a "piranha solution" (1:2 v/v H_2SO_4 (98%)/H_2O_2 (30 wt %) mixture) at 80 °C for 20 min, rinsed in Milli-Q water, and dried by spinning at 4000 rpm for a few seconds in a clean room environment. Separate XRR experiments[42] have shown that this procedure efficiently removes organic contaminants without introducing measurable roughening of the surface. This washing procedure has been reported elsewhere[30,43] to produce a highly hydrophilic surface by leaving on the silicon substrate a 10−20 Å thick silicon oxide (Si/SiO_x) layer. Some silicon pieces were then coated by 300 Å thick evaporated amorphous carbon (a-C) films. These were prepared using the electron-bombardment method[44] with a EVM030 vacuum coating unit from Balzers (pressure below 10^{-5} mbar, incident current intensity equal to 50 mA, and sample surface to source distance equal to 15 cm). The obtained carbon films, too thin to show a color perceptible to the eye, were of sufficient quality to be characterized by XRR.

Polymers. The synthesis and bulk characterization of the diblock copolymers used in this study have been described in detail in refs 36 and 37. These copolymers basically consist of strongly asymmetric chlorinated polybutadiene-*b*-polystyrene hydrogen-terminated diblock copolymers (P(CB-*b*-S)), with a PCB volume fraction of about 10%. They were obtained by selective chlorination of the polybutadiene (PB) segment of polybutadiene-*b*-polystyrene anionic block copolymers which were initiated by *sec*-butyllithium and terminated in methanol. Their chemical architecture can be summarized by the notation of Figure 1.[37] Chlorination of the PB segment is not complete; a degree of chlorination of 84% was determined by size-exclusion chromatography (SEC) and elemental analysis.[37] The end-tagged polystyrene used in this study is characterized with reference to Figure 1 by $m \approx 26$, $n \approx 4$, and $p \approx 450$.[37] The parent homopolymers were also used in this study. Chlorinatd polybutadiene (homo-CPB) with $\bar{M}_n = 33\,500$ and $\bar{M}_w/\bar{M}_n = 1.05$ was obtained from the chlorination of a homodisperse PB ($\bar{M}_n = 16\,900$, $\bar{M}_w/\bar{M}_n = 1.03$).[19] Homodisperse ($\bar{M} = 96\,400$ and $\bar{M}_w/\bar{M}_n < 1.05$) H-terminated polystyrene (homo-PS) was obtained from Waters.

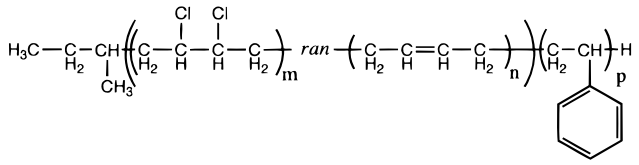

Figure 1. Schematic of the P(CB-*b*-S) copolymer used in this study ($m \approx 26$, $n \approx 4$, $p \approx 450$).

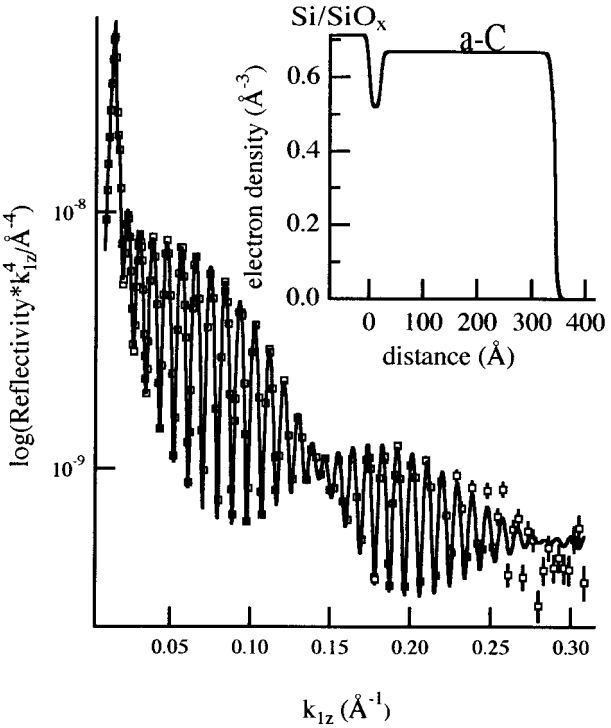

Figure 2. Reflectivity curve of an a-C film evaporated onto a silicon wafer. Solid line is the best fit calculated with the electron density profile shown in the inset.

Polymer Deposition. Thin films of the asymmetric diblock and its parent homopolymers were deposited onto the substrates by spin-coating in toluene, directly after cleaning the substrates. The polymer solution concentration (1% w/v), rotation speed (4000 rpm), and acceleration (20 000 rpm/s) were adjusted to produce samples with polymer film thicknesses of approximately 300 Å for the predominantly styrene polymers and 250 Å for homo-CPB. Films may be considered as three-dimensional when their thickness d is much larger than the unperturbed radius of gyration R_g of the chains,[45] which is the case here ($d/R_g \approx 3.5$).[46] The samples were characterized before and after annealing at 150 °C in a vacuum oven for 8 h. No significant change by XRR, DSIMS, or XPS was observed beyond this time period. This annealing procedure was adopted to limit oxidation and dehydrochlorination of the samples during annealing. Moreover, absence of film dewetting or free surface roughening upon annealing was checked by optical microscopy and XRR.

Results

Thin Carbon Films. A typical X-ray reflectivity profile for a a-C film deposited onto Si/SiO_x is shown in Figure 2 as a function of the half wave vector transfer k_{1z} ($k_{1z} = 2\pi/\bar{\lambda} \sin \theta^0$, with $\bar{\lambda}$ being the wavelength and θ^0 half the scattering angle). The XRR profile is essentially made of a high-frequency oscillation characteristic of the thickness of the carbon film superposed onto a low-frequency oscillation corresponding to dis-

tances of about 22 Å between two interfaces (for the data shown here) in the derivative of the electron density profile. These features are indeed observable in the model giving the best agreement between experimental data and calculated reflectivities (Figure 2). A strong drop of density is observed at the Si/SiO_x interface over a distance of about 22 Å. It is not clear whether this dip, whose shape changed from sample to sample and whose width varied between 20 and 30 Å, is inherent to the deposition process or due to some organic contamination occurring during the deposition of the a-C film. The roughnesses found are consistent with surface roughness values previously determined by XRR for carbon films sputtered in Ar.[47] Amorphous carbon is generally described as disordered graphitic islands of 15−20 Å diameter bounded by sp^3 sites.[48,49] Our a-C thin layers have an electron density of 0.63 ± 0.03 Å^{-3}, which is near the theoretical value for hexagonal graphite (0.6823 Å^{-3}) computed from published crystallographic data.[50] The density of amorphous carbon films has been reported,[51] ranging from 0.42 to 0.67 Å^{-3} depending on the preparation technique, thickness, and characterization method used. Our densities values are actually comparable to density values for sputtered carbon films with similar thickness determined by XRR.[47] XPS survey scan (not shown) reveals a slight oxidation of the carbon surface. The surface oxygen content was estimated around 7 at. %.

Thin Polymers Films. (1) XRR. A representative selection of curves of log(reflectivity·k_{1z}^4) vs k_{1z} for P(CB-*b*-S) deposited onto Si/SiO_x and a-C, before and after annealing at 150 °C for 8 h, are shown in Figures 3 and 4, respectively. Also shown in these figures are the computed electron density profiles and computed reflectivities. In all cases, we had to introduce a drop in the density profiles of the films near the solid substrates to reproduce fully the data. This drop was already discussed elsewhere[36,52] and was observed for a series of homopolymers interacting weakly with Si/SiO_x substrates, including pure homo-PS. Although the origin of this dip is still uncertain, a detailed analysis of the Patterson functions has demonstrated that this feature is not an artifact arising from the data analysis.[52] In addition, it has been shown that, for polymer interacting more strongly with Si/SiO_x, a density increase is measured at interfaces instead of a depletion,[52] ruling out the drop being due to contamination of the substrate before spin-coating. In the present context, we simply note that for our end-tagged polystyrenes P(CB-*b*-S) the presence of this electron density dip prevents to accurately decide from XRR experiments whether any preferential segregation occurs after annealing. Therefore, DSIMS and XPS experiments were performed to obtain this information.

(2) XPS. With its sampling depth of a few tens of angstroms, XPS is perfectly suited to provide information on the composition of the near free surface region. Parts a and b of Figure 5 show the XPS survey scans for 300 Å thick P(CB-*b*-S) films deposited onto respectively Si/SiO_x and a-C and probed before and after annealing at 150 °C for 8 h. Apart from carbon and chlorine contributions expected from the polymer architecture given in Figure 1, trace contributions from oxygen and silicon are observed.

A proper analysis of the small peaks associated with chlorine, oxygen, and silicon requires multiple scanning of a small region centered on the line of interest. From

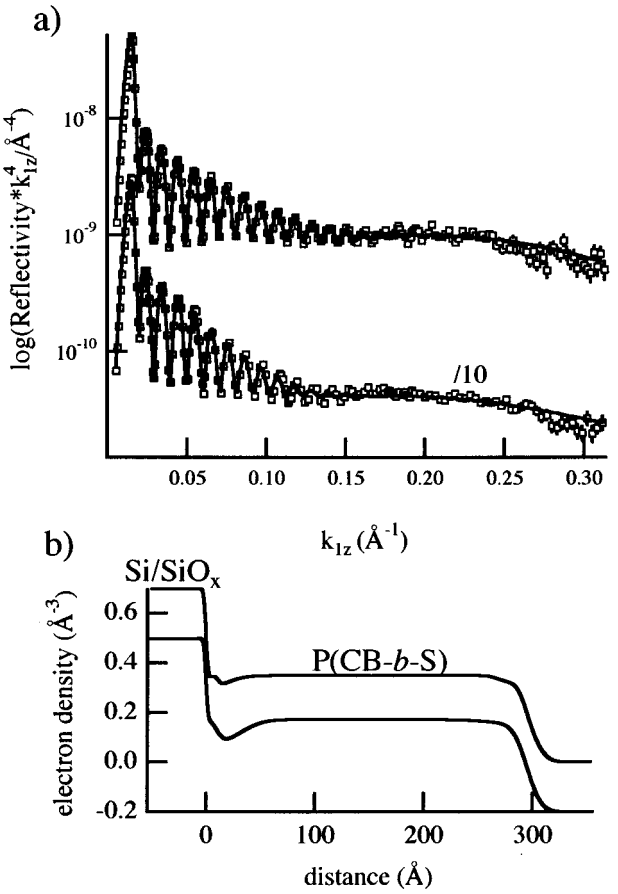

Figure 3. (a) Reflectivity curves for a P(CB-*b*-S) film spin-coated onto a silicon wafer. Solid lines are best fits calculated with the electron density profiles shown in (b). Upper lines, before annealing; bottom lines, after annealing (vertical shift: −0.2 Å^{-3}).

these high-resolution scans, atomic surface compositions (excluding H which is not detected by XPS) expressed in at. % can be derived and are given in Table 1. (For silicon and chlorine, the 2p peaks were chosen because of their higher sensitivity factor.) The error limits given come from the dispersion of results obtained from different zones taken on a same sample surface and from different samples. Because of the relatively large uncertainties on some intensities, only general trends will be discussed in this study. The positions of the silicon lines (101.5 ± 0.5 eV for Si(2p) and 152.2 ± 0.5 eV for Si(2s)) are characteristic of Si−O groups. The fact that these lines are observed for both substrates rules out the possibility of some influence of the underlying silicon wafer and rather suggests the presence of slight but inevitable PDMS contamination at the surface. Despite large uncertainties on the surface compositions, the extent of surface oxygen for the unannealed samples (≈1 at. %) cannot be explained solely by the PDMS contamination as then the silicon and oxygen should be 1:1. The intensity of the O(1s) line at 532 eV is difficult to interpret as this line may be the result of many factors; oxidation products, residual oxygen-containing molecules in the spectrometer, and/or adventitious oxygen from impurities. While the two latter possibilities cannot be excluded, slight oxidation of the CPB marker is highly probable. Low oxygen contents were detected in homo-CPB by infrared spectroscopy and elemental analysis,[37] and significant O^- currents were detected in the P(CB-*b*-S) and homo-CPB layers by

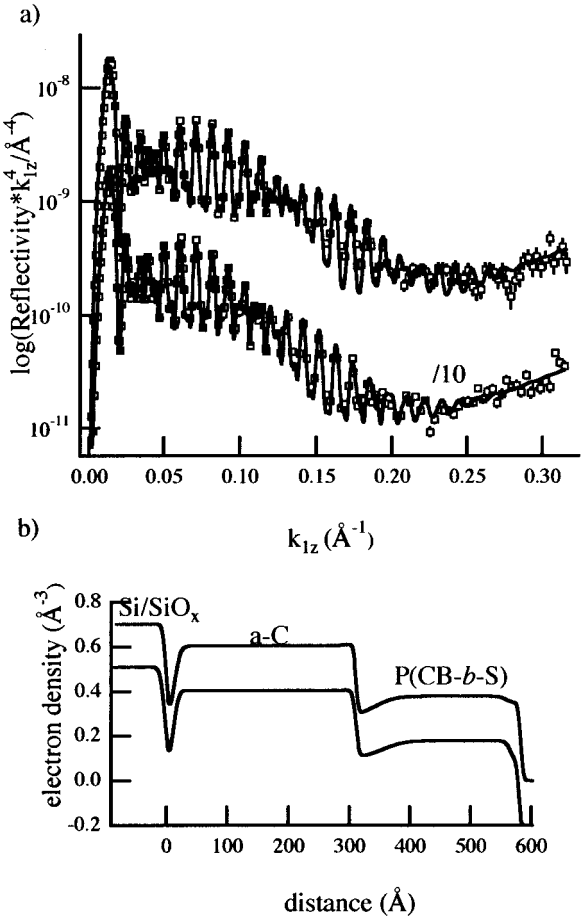

Figure 4. (a) Reflectivity curves for a P(CB-*b*-S) film spin-coated onto an a-C film evaporated itself onto a silicon wafer. Solid lines are best fits calculated with the electron density profiles shown in (b). Upper lines, before annealing; bottom lines, after annealing (vertical shift: −0.2 Å^{-3}).

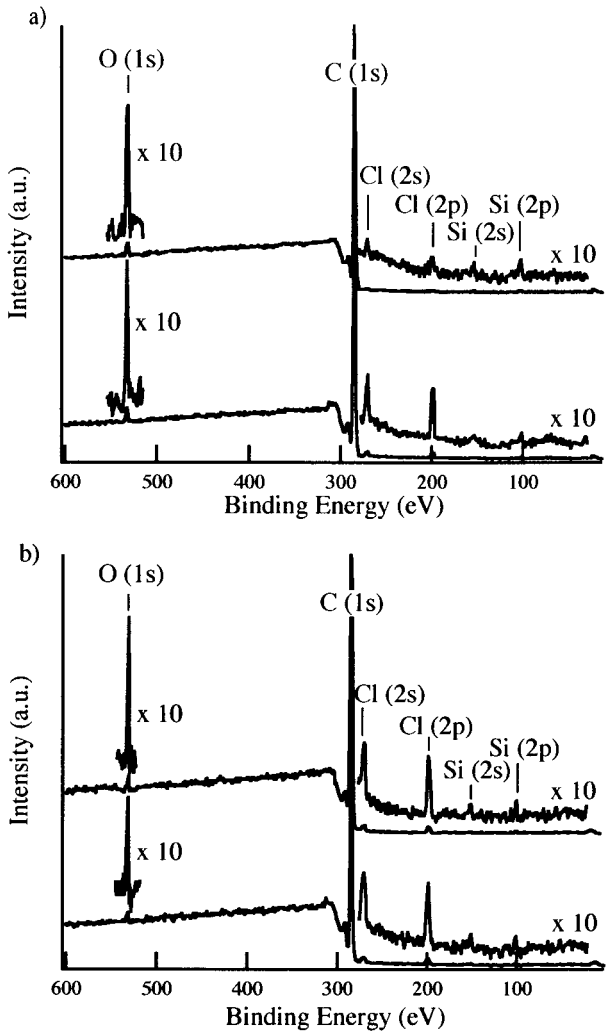

Figure 5. XPS survey scans of a 300 Å thick P(CB-*b*-S) film deposited onto Si/SiO$_x$ (a) and a-C (b). Below, before annealing; above, after annealing. Intensity above 600 eV is not shown here since it is featureless except for the presence of a very small O-KLL signal.

DSIMS (see below). In the present case, a precise determination of all these effects is impossible.

The presence of chlorine is shown by the presence of its two lines: Cl(2p) at 200.3 ± 0.9 eV and Cl(2s) at 271.0 ± 0.6 eV. Its surface atomic content before annealing is slightly lower than what is expected from the stoichiometry proposed in Figure 1. This effect, which is hardly significant, might be due to the previously discussed presence of a contamination layer on the samples. Dehydrochlorination due to heating of the surface by the X-ray source has been previously reported in XPS experiments on PVC.[53] The absence of significant chlorine release in our experiments has been checked by determining the surface chlorine content from survey scans as a function of the accumulation time. No clear evolution appeared within 120 min, which is approximately the total exposure time during which a sample area is probed.

The annealing process did not lead to the appearance of new elements or increase of the silicon signals intensity in the survey spectra (see Figure 5), indicating that no additional contamination took place in the vacuum oven and confirming the absence of dewetting upon annealing. After annealing P(CB-*b*-S) deposited onto Si/SiO$_x$, the most significant difference (see Figure 5 and Table 1) is the large attenuation of the Cl(2s) and Cl(2p) contributions. The chlorine depletion after annealing is clearly evidenced on the high-resolution scans given in Figure 6. By contrast, when deposited onto a-C, no significant variation can be seen in the Cl(2p) and Cl(2s) lines (see Figure 7). Our XPS experiments thus reveal that chlorine depletion at the free interface occurs or not, depending on the nature of the substrate onto which the thin diblock film was deposited. To confirm these results, a DSIMS depth profiling of our films was performed.

(3) DSIMS. The C$^-$, O$^-$, Si$^-$, and Cl$^-$ secondary currents measured for a 300 Å thick P(CB-*b*-S) film deposited onto Si/SiO$_x$ before and after annealing at 150 °C for 8 h are plotted in relative units vs the primary ion fluence in Figure 8, a and b, respectively. Figure 9a,b is a similar figure drawn for the P(CB-*b*-S) film deposited onto a-C. Before drawing any elaborate conclusion with respect to the observed variations of secondary currents with depth, it is important to pay attention to a series of experimental artifacts that are inevitably present in DSIMS results. The position of the polymer/solid substrate interface can be easily determined in the present case by the concomitant sudden increase (decrease) of Si$^-$ and O$^-$ (C$^-$) currents. Even with step function profiles, a broadening of the profiles is expected as observed due to a complex interplay between atomic mixing and instrumental effects.[54] Apart from inducing a loss of surface material (sput-

Table 1. XPS Atomic Surface Compositions (Excluding H Which Is Not Detected by XPS) of P(CB-*b*-S) Deposited onto Si/SiO_x and a-C, before and after Annealing

sample	at. % C (98.62)[a]	at. % O (0)[a]	at. % Cl (1.38)[a]	at. % Si (0)[a]
P(CB-*b*-S)/(Si/SiO_x) unannealed	98.0 ± 0.7	0.9 ± 0.3	1.0 ± 0.3	0.1 ± 0.1
P(CB-*b*-S)/(Si/SiO_x) annealed	99.2 ± 0.5	0.6 ± 0.3	0.1 ± 0.1	0.1 ± 0.1
P(CB-*b*-S)/a-C unannealed	98.0 ± 0.7	0.8 ± 0.3	1.1 ± 0.3	0.1 ± 0.1
P(CB-*b*-S)/a-C annealed	97.9 ± 0.8	1.1 ± 0.4	0.9 ± 0.3	0.1 ± 0.1

[a] Values based upon the known stoichiometry.

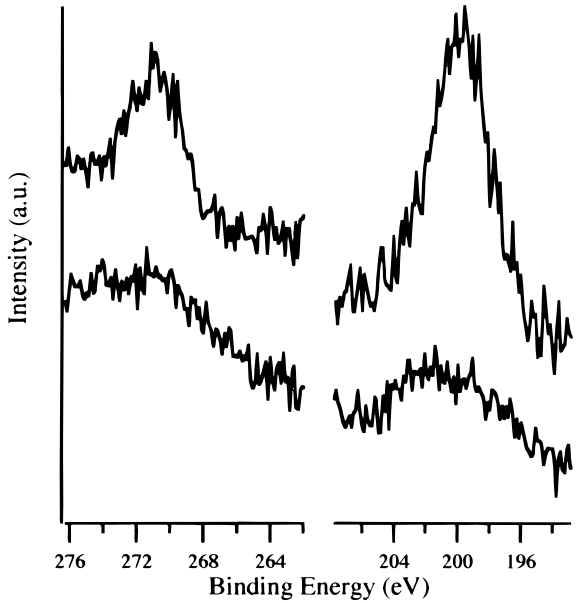

Figure 6. XPS Cl(2s) (left) and Cl(2p) (right) spectra of a 300 Å thick P(CB-*b*-S) film deposited onto Si/SiO_x. Above, before annealing; below, after annealing. Spectra are normalized for constant total area under peaks.

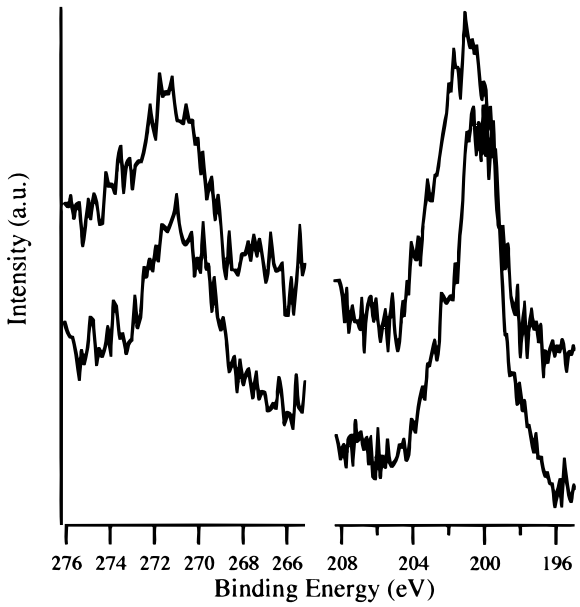

Figure 7. XPS Cl(2s) (left) and Cl(2p) (right) spectra of a 300 Å thick P(CB-*b*-S) film deposited onto a-C. Above, before annealing; below, after annealing. Spectra are normalized for constant total area under peaks.

tering), the impingement of energetic ions into the surface layer during SIMS involves changes in the structure of the target (atomic mixing, preferential sputtering).[55] An atom originally collided by a primary ion is recoiled and produces successive displacements of neighboring atoms, inducing a collision cascade.[56] Instrumental effects include factors depending on the particular spectrometer used, ion bombardment conditions, and sample charging.[56] Often cited as a dominant contribution to profile broadening,[55] the initial sample surface roughness should in our case be of little influence.

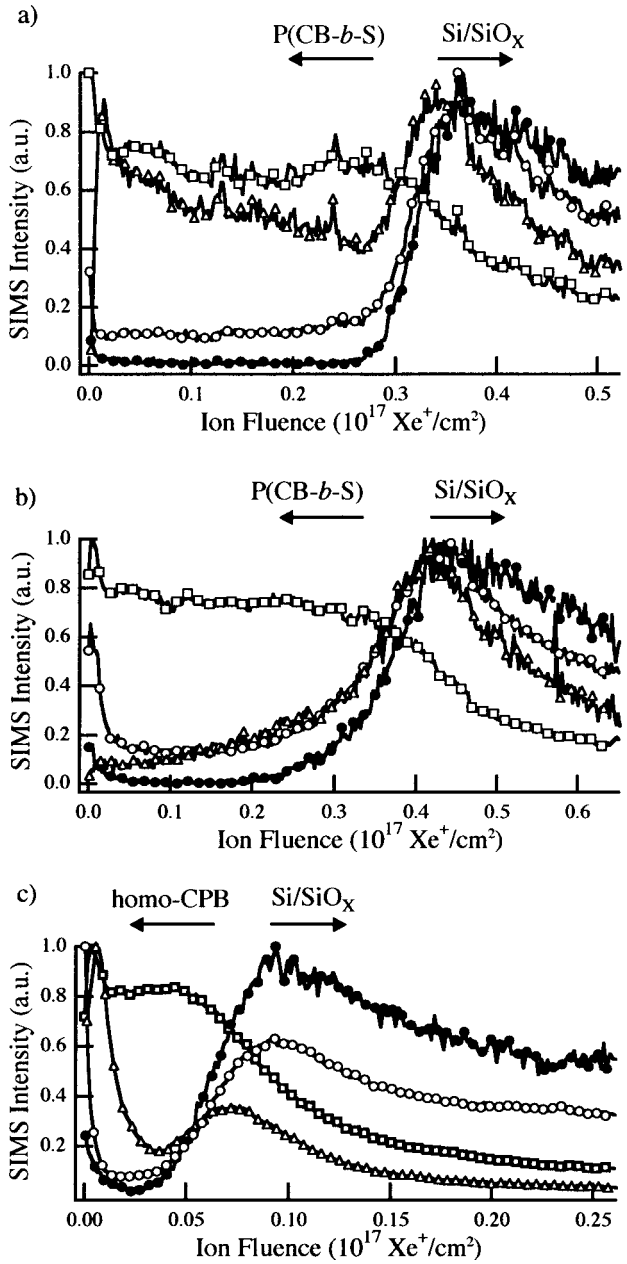

Figure 8. Normalized C^- (□), O^- (○), Si^- (●), and Cl^- (△) DSIMS profiles for (a) a 300 Å thick P(CB-*b*-S) film deposited onto Si/SiO_x before annealing (maximum number of recorded counts: C^- (8984), O^- (2782), Si^- (849), and Cl^- (1416)); (b) same film after annealing (C^- (17931), O^- (2991), Si^- (563), and Cl^- (778)); (c) a 250 Å thick homo-CPB film deposited onto Si/SiO_x after annealing (C^- (25 451), O^- (16 904), Si^- (1008), and Cl^- (16 074)). Markers are representative experimental points given by the solid lines.

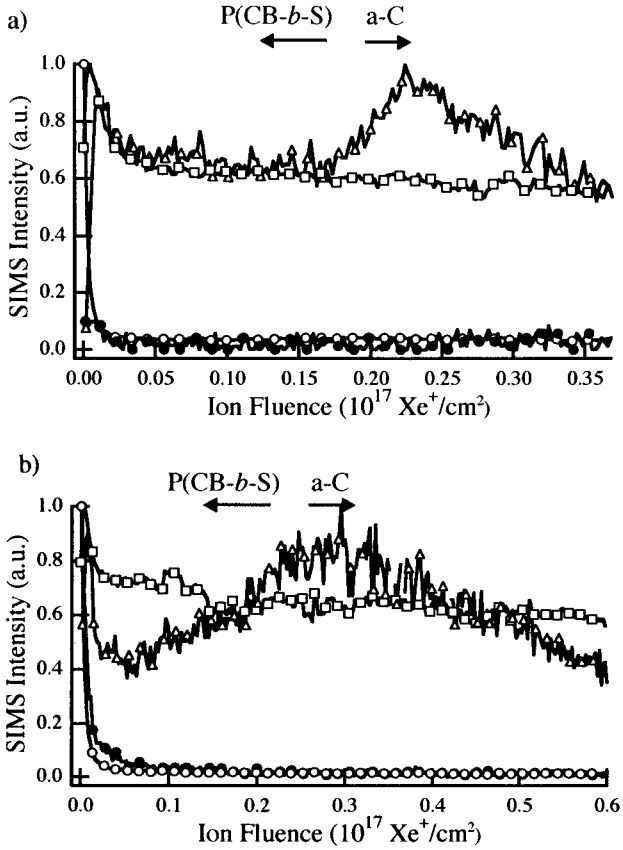

Figure 9. Normalized C^- (□), O^- (○), Si^- (●), and Cl^- (△) DSIMS profiles for (a) a 300 Å thick P(CB-*b*-S) deposited onto a-C before annealing (maximum number of recorded counts: C^- (21 131), O^- (8385), Si^- (612), and Cl^- (891)); (b) same film after annealing (C^- (17 666), O^- (19 302), Si^- (508), and Cl^- (397)). Numbers in parentheses are the maximum number of recorded counts. Markers are representative experimental points which are given by the solid lines.

Large variations of secondary currents are detected at the free interface, due to the nonuniformity of the etching rate in the first few tens of angstroms of the film.[9] Some authors avoided this effect by adding a sacrificial layer atop the film to be analyzed.[16,57] We did not resort to this, since the surface composition of the film was already known by XPS.

The large increase of the Cl^- current observed at the P(CB-*b*-S)/substrate interface before and after annealing is present for all systems whatever the substrate used. It is also observed when homo-CPB is deposited onto the same substrates (see Figure 8c for homo-CPB deposited onto Si/SiO_x). It is therefore not related to any preferential segregation of chlorine species but more probably to a matrix effect. Another feature worth mentioning in Figure 8c is the high sputtering rate observed when homo-CPB is bombarded compared to that found for predominantly styrene polymers in comparable experimental conditions. A primary ion fluence of $(0.25-0.35) \times 10^{17}$ Xe^+/cm^2 was needed for a 300 Å thick P(CB-*b*-S) film to be completely sputtered off the substrate (Figures 8a,b and 9) while only $\sim 0.05 \times 10^{17}$ Xe^+/cm^2 was needed for a homo-CPB film of comparable initial thickness ($\sim$250 Å). This observation leads us to think that extensive dehydrochlorination of homo-CPB occurred during analysis. Similar conclusions were drawn from results obtained with chlorinated polypropylene.[58] Significant but small oxygen amounts were detected in the homo-CPB and P(CB-*b*-S) (Figures 8a,b and 9) films. This is in agreement with the slight oxidation observed for homo-CPB by infrared spectroscopy and elemental analysis.

We now turn to significant effects of annealing on the depth profiles. After annealing the film on Si/SiO_x for 8 h at 150 °C, the only significant change observed is in the Cl^- profile: a large depletion of chlorine is now present, starting from the air interface toward deep into the film. Concerning the film deposited on a-C, the C^- current is seen to be identical for both the polymer and a-C; consequently, the only feature that could reveal the presence of the P(CB-*b*-S)/a-C interface during the sputtering process is the already mentioned peak (Figure 9) in the Cl^- current. Compared to the chlorine depletion observed after annealing starting from the air interface for P(CB-*b*-S) deposited onto Si/SiO_x (Figure 8a,b), the Cl^- profiles before and after annealing here show very little variation if any when one considers the reproducibility of the measurements.

Clear differences are thus detected by DSIMS in the way Cl^- profiles vary upon annealing, depending on the substrate considered. Assuming that the chlorine distribution is homogeneous in the spin-coated film before annealing, DSIMS indicates that the annealing does not change significantly this homogeneous distribution for films on a-C substrates, while a strong chlorine depletion is detected starting from the air interface for films on Si/SiO_x. These observations are in perfect agreement with the XPS results, which indicated a depletion of Cl at the free interface upon annealing the film deposited on Si/SiO_x, while no variations could be detected for the film deposited onto a-C. These observations can only be explained by a preferential accumulation of chlorinated butene segments at the Si/SiO_x interface upon annealing, with in turn a depletion at the air interface resulting from the small film thickness. The direct observation of the accumulation at the Si/SiO_x interface is however not possible, given the perturbations in the Cl^- profiles occurring near the substrate interface as reported above.

Discussion

From the polymer architecture given in Figure 1, the chlorine depletion upon annealing observed when P(CB-*b*-S) is deposited onto Si/SiO_x may a priori be due either to a preferential adsorption of the styrene segments at the polymer/air interface or to a preferential accumulation of the CPB segments at the polar Si/SiO_x surface or to both. However, the absence of chlorine depletion when an apolar substrate is used (Figures 5b, 7, and 9) clearly indicates that a preferential segregation of the styrene segments toward the free surface plays, if any, only a minor role in the chlorine depletion evidenced in Figures 5a, 6, and 8. From eq 1, the absence of any preferential segregation of the PS or CPB block to the free surface would mean that the net interaction energies experienced by two styrene segments and by two chlorinated butene segments in the bulk are comparable. This is consistent with estimations of the cohesive energy densities at 20 °C for polystyrene and poly(vinyl chloride) made by the Hoftyzer−Van Krevelen method.[59] By taking experimental molar volumes at 20 °C,[59] identical values within the error of the method (10%)[59] are obtained for PS (363 J/cm^3) and PVC (389 J/cm^3).

The preferential adsorption of the CPB marker at polar surfaces should be governed by a minimization of the interfacial polymer/substrate energy $\gamma_{P,S}$. Estimation

of the interfacial energy reduction implied by a segregation of CPB at a substrate S where S is either Si/SiO_x or a-C

$$\Delta\gamma_S = \gamma_{CPB,S} - \gamma_{PS,S} \quad (3)$$

can be performed using the Dupré equation[60] giving the interfacial energy $\gamma_{P,S}$ in terms of surface energies of polymer P and substrate S (γ_P and γ_S) and the work of adhesion between polymer and substrate $W_{P,S}$

$$\gamma_{P,S} = \gamma_P + \gamma_S - W_{P,S} \quad (4)$$

Splitting the work of adhesion into a term $W^d_{P,S} = 2(\gamma^d_P\gamma^d_S)^{1/2}$ corresponding to long-range dispersive interactions and a term referring to all nondispersive interactions $W^{nd}_{P,S} = 2(\gamma^{nd}_P\gamma^{nd}_S)^{1/2}$, $\gamma_{P,S}$ is rewritten in terms of dispersive (γ^d) and nondispersive (γ^{nd}) surface energies ($\gamma = \gamma^d + \gamma^{nd}$)[61]

$$\gamma_{P,S} = \gamma_P + \gamma_S - 2(\gamma^d_P\gamma^d_S)^{1/2} - 2(\gamma^{nd}_P\gamma^{nd}_S)^{1/2} \quad (5)$$

Hence,

$$\Delta\gamma_S = \gamma_{CPB} - \gamma_{PS} - 2(\gamma^d_S)^{1/2}((\gamma^d_{CPB})^{1/2} - (\gamma^d_{PS})^{1/2}) - 2(\gamma^{nd}_S)^{1/2}((\gamma^{nd}_{CPB})^{1/2} - (\gamma^{nd}_{PS})^{1/2}) \quad (6)$$

Assuming once again that homo-CPB has the same physicochemical properties as PVC, $\gamma^d_{CPB} \approx \gamma^d_{PVC} = 41.5$ mJ/m^2 [62] and $\gamma^{nd}_{CPB} \approx \gamma^{nd}_{PVC} = 9$ mJ/m^2.[63] Similarly for PS, $\gamma^d_{PS} = 42$ mJ/m^2 [62] and $\gamma^{nd}_{PS} = 4.1$ mJ/m^2.[63] By using the dispersive ($\gamma^d_{a-C} = 46.3$ mJ/m^2) and nondispersive parts ($\gamma^{nd}_{a-C} = 5.5$ mJ/m^2) of the surface energy for a-C sputtered on borosilicate glass recently determined by a surface force apparatus,[64] we find $\Delta\gamma_{a-C} = 0.46$ mJ/m$^2 \approx 0$ mJ/m^2. Published values of total surface energies for a silicon oxide surface range from 129 to 259 mJ/m^2,[65] depending on the silanol-to-siloxane ratio. On the other hand, the dispersion component of the surface tension for silica has been measured by gas adsorption[66] ($\gamma^d = 76$ mJ/m^2). Putting these values in eq 6, we find -20.6 mJ/m$^2 \le \Delta\gamma_{Si/SiO_x} \le -8.8$ mJ/m^2 and $\Delta\gamma_{Si/SiO_x} \ll \Delta\gamma_{a-C}$. Hence, despite the large uncertainties in the surface energies for the silicon oxide surface, these estimations clearly show that a preferential adsorption of the chlorinated segments toward the Si/SiO_x surface is energetically highly favored, the energetic driving force disappearing for the a-C surface.

Moreover, eq 6 shows that energetically driven segregation toward an a-C surface will be weak for any pair of polymers having comparable dispersive surface energies since γ^{nd}_{a-C} is very small as compared to γ^d_{a-C}. As many polymers (polystyrene, polyamides, poly(methyl methacrylate), etc.) have their γ^d around 40 mJ/m^2,[62] the a-C surface thus seems to be an appropriate choice for many multicomponent thin polymer films (tagged polymers, copolymers, blends) whenever preferential interactions with substrate are to be avoided. By contrast, the nondispersive component of the surface energy of Si/SiO_x is much larger than γ^{nd}_{a-C}. Consequently, the silicon oxide surface preferentially attracts the more polar segments, in our case the CPB block whose polarity is largely due to the inductive effects of the chlorine atoms. Our previous considerations neglect the always possible existence of specific interactions between polymer segments and the surfaces. For instance, silicon dioxide is considered as an acidic surface, due to the presence of silanol moieties on the surface. For polymers capable of forming H-bonds with the surface, this should certainly be taken into account when establishing the overall energetic balance. However, these complications are not important for the presently reported system.

Conclusions

An experimental study of segregation phenomena in thin films of a strongly asymmetric diblock P(CB-*b*-S) copolymer was carried out. In bulk samples, the short CPB blocks do not phase segregate at the selected annealing temperature (150 °C) despite the existing incompatibility between the two blocks. By contrast, we conclude from DSIMS and XPS observations that a preferential segregation of the CPB short block toward polar surfaces occurs at this temperature. As the surface polar character decreases, this segregation tendency decreases as well, indicating that the localization of the short block in these systems is mainly governed by energetic factors, the entropic contribution being negligible. This is similar to what was observed previously for more symmetric diblock copolymers and for end-tagged polymer chains, indicating that energetic effects are dominating the segregation behavior over the whole range of diblock composition. In XRR studies, these relatively small effects are hidden by density perturbations near the solid substrate which are much stronger than the electron density variations due to segregation effects.

Acknowledgment. Anionic polymerizations were performed at the Centre d'Etude et de Recherche sur les Macromolécules (CERM) of the University of Liège, Belgium. The authors are especially grateful to Prof. R. Jérôme for his hospitality and helpful suggestions. We are also indebted to Prof. P. Dubois (University of Mons-Hainaut, Belgium) for valuable comments and advice in polymer syntheses, to M. Genet (UCL) for technical assistance in the XPS experiments, and to Dr. X. Arys (UCL) for fruitful discussions about XRR analysis. C. Poleunis and part of this work are supported by the PAI-IUAP P4/10 Belgium federal research program on Reduced Dimensionality Systems.

References and Notes

(1) Hasegawa, H.; Hashimoto, T. *Macromolecules* **1985**, *18*, 589.
(2) Fredrickson, G. H. *Macromolecules* **1987**, *20*, 2535.
(3) Anastasiadis, S. H.; Russell, T. P.; Satija, S. K.; Majkrzak, C. F. *Phys. Rev. Lett.* **1989**, *62*, 1852.
(4) Green, P. F.; Christensen, T. M.; Russell, T. P.; Jerome, R. *J. Chem. Phys.* **1990**, *92*, 1478.
(5) Green, P. F.; Christensen, T. M.; Russell, T. P. *Macromolecules* **1991**, *24*, 252.
(6) Russell, T. P.; Menelle, A.; Anastasiadis, S. H.; Satija, S. K.; Majkrzak, C. F. *Macromolecules* **1991**, *24*, 6263.
(7) Menelle, A.; Russell, T. P.; Anastasiadis, S. H.; Satija, S. K.; Majkrzak, C. F. *Phys. Rev. Lett.* **1992**, *68*, 67.
(8) Lambooy, P.; Russell, T. P.; Kellogg, G. J.; Mayes, A. M.; Gallagher, P. D.; Satija, S. K. *Phys. Rev. Lett.* **1994**, *72*, 2899.
(9) Sikka, M.; Singh, N.; Bates, F. S.; Karim, A.; Satija, S.; Majkrzak, C. F. *J. Phys. II* **1994**, *4*, 2231.
(10) Clarson, S. J.; Stuart, J. O.; Selby, C. E.; Sabata, A.; Smith, S. D.; Ashraf, A. *Macromolecules* **1995**, *28*, 674.
(11) Mansky, P.; Russell, T. P.; Hawker, C. J.; Mays, J.; Cook, D. C.; Satija, S. K. *Phys. Rev. Lett.* **1997**, *79*, 237.
(12) Thomas, H. R.; O'Malley, J. J. *Macromolecules* **1979**, *12*, 323.
(13) Thomas, E. L.; Kinning, D. J.; Alward, D. B.; Henkee, C. S. *Macromolecules* **1987**, *20*, 2934.
(14) Henkee, C. S.; Thomas, E. L.; Fetters, L. J. *J. Mater. Sci.* **1988**, *23*, 1685.

(15) Karim, A.; Singh, N.; Sikka, M.; Bates, F. S.; Dozier, W.; Felcher, G. P. *J. Chem. Phys.* **1994**, *100*, 1620.
(16) Liu, S.; Zhao, W.; Zheng, X.; King, A.; Singh, A.; Rafailovich, M. H.; Sokolov, J.; Dai, K. H.; Kramer, E. J.; Schwarz, S. A.; Gebizlioglu, O.; Sinha, S. K. *Macromolecules* **1994**, *27*, 4000.
(17) van Dijk, M. A.; van den Berg, R. *Macromolecules* **1995**, *28*, 6773.
(18) Radzilowski, L. H.; Carvalho, B. L.; Thomas, E. L. *J. Polym. Sci., Part B: Polym. Phys.* **1996**, *34*, 3081.
(19) Iyengar, D. R.; Perutz, S. M.; Dai, C.-A.; Ober, C. K.; Kramer, E. J. *Macromolecules* **1996**, *29*, 1229.
(20) Bottino, F. A.; Di Pasquale, G.; Pollicino, A.; Pilati, F.; Toselli, M.; Tonelli, C. *Macromolecules* **1998**, *31*, 7814.
(21) Wool, R. P. *Polymer Interfaces, Structure and Strength*; Hanser/Gardner Publications: Cincinnati, OH, 1995; Chapters 11 and 12.
(22) Wang, Y.; Winnig, M. A. *J. Phys. Chem.* **1993**, *97*, 2507.
(23) Bitsanis, I.; Hadziioannou, G. *J. Chem. Phys.* **1990**, *92*, 3827.
(24) Kumar, S. K.; Vacatello, M.; Yoon, D. Y. *J. Chem. Phys.* **1988**, *89*, 5206.
(25) Mansfield, K. F.; Theodorou, D. N. *Macromolecules* **1990**, *23*, 4430; **1991**, *24*, 4295.
(26) Theodorou, D. N. *Macromolecules* **1988**, *21*, 1391; **1989**, *22*, 4578; **1989**, *22*, 4589.
(27) Affrossman, S.; Hartshorne, M.; Jérôme, R.; Pethrick, R. A.; Petitjean, S.; Rei Vilar, M. *Macromolecules* **1993**, *26*, 6251.
(28) Agrawal, G.; Wool, R. P.; Dozier, W. D.; Felcher, G. P.; Russell, T. P.; Mays, J. W. *Macromolecules* **1994**, *27*, 4407.
(29) Zhao, W.; Zhao, X.; Rafailovich, M. H.; Sokolov, J.; Composto, R. J.; Smith, S. D.; Satkowski, M.; Russell, T. P.; Dozier, W. D.; Mansfield, T. *Macromolecules* **1993**, *26*, 561.
(30) Elman, J. F.; Johs, B. D.; Long, T. E.; Koberstein, J. T. *Macromolecules* **1994**, *27*, 5341.
(31) Hariharan, A.; Kumar, S. K.; Russell, T. P. *J. Chem. Phys.* **1993**, *98*, 4163; **1993**, *99*, 656.
(32) Hariharan, A.; Kumar, S. K.; Russell, T. P. *Macromolecules* **1991**, *23*, 3584; **1991**, *24*, 4909.
(33) Kumar, S. K.; Russell, T. P. *Macromolecules* **1991**, *24*, 3816.
(34) Jones, R. A. L.; Kramer, E. J.; Rafailovich, M. H.; Sokolov, J.; Schwartz, S. A.; Leibler, L. *Phys. Rev. Lett.* **1989**, *62*, 280.
(35) Bates, F. S.; Wignall, G. D. *Phys. Rev. Lett.* **1986**, *57*, 1429.
(36) Stone, V. W. PhD Thesis, UCL, 1999.
(37) Stone, V. W.; Jonas, A. M.; Legras, R.; Dubois, P.; Jérôme, R. *J. Polym. Sci., Polym. Chem. Ed.* **1999**, *374*, 233.
(38) Parrat, G. *Phys. Rev.* **1954**, *95*, 359.
(39) Pedersen, J. K.; Hamley, I. W. *J. Appl. Crystallogr.* **1994**, *27*, 36.
(40) Russell, T. P. *Mater. Sci. Rep.* **1990**, *5*, 186.
(41) Siordia, R. *Note Surf. Sci. Instrum.* **1987**, Nov 19.
(42) Stone, V. W., unpublished results.
(43) Carim, A. H.; Dovek, M. M.; Quate, C. F.; Sinclair, R.; Vorst, C. *Science* **1987**, *237*, 630.
(44) Bell, A. E.; Pritchard, J.; Sykes, K. W. *Proceedings 2nd Conference on Industrial Carbon and Graphite*; Society of the Chemical Industry: London, 1966.
(45) Shuto, K.; Oishi, Y.; Kajiyama, T.; Han, C. C. *Polym. J.* **1993**, *25*, 291.
(46) R_g was estimated using the relation $R_g = (Pb^2/6)^{1/2}$, P being the degree of polymerization and b the statistical segment length. Taking 6.81 Å for the statistical segment length of PS (Sato, M.; Koshiishi, Y.; Asahina, M. *J. Polym. Sci., Part B, Polym. Lett. Ed.* **1963**, *1*, 233) and the statistical segment length of PVC for CPB (7.16 Å, same reference), we get R_g = 85 Å for homo-PS, 68 Å for homo-CPB, and 63 Å for P(CB-*b*-S) using the architecture presented in Figure 1.
(47) Toney, M. F.; Brennan, S. *Phys. Rev. B* **1989**, *66*, 1861.
(48) Robertson, J.; O'Reilly, E. P. *Phys. Rev. B* **1987**, *6*, 2946.
(49) Beeman, D.; Silverman, J.; Lynds, R.; Anderson, M. R. *Phys. Rev. B* **1984**, *30*, 870.
(50) Kelly, B. T. *Physics of Graphite*; Applied Science: London, 1981.
(51) Tsai, H. C.; Bogy, D. B. *J. Vac. Sci. Technol. A* **1987**, *5*, 3287.
(52) Bollinne, C.; Stone, V. W.; Jonas, A. M. *Macromolecules* **1999**, *32*, 4719.
(53) Busscher, H. J.; Hoogsteen, W.; Dijkema, L.; Sawatsky, G. A.; Van Pelt, A. W. J.; De Jong, H. P.; Challa, G.; Arends, J. *Polym. Commun.* **1985**, *26*, 252.
(54) Whitlow, S. J.; Wool, R. P. *Macromolecules* **1991**, *24*, 5926.
(55) Benninghoven, A.; Rudenauer, F. G.; Werner, H. W. *Secondary Ion Mass Spectrometry, Chemical Analysis Series 86*; John Wiley and Sons: New York, 1987.
(56) Magee, C. W.; Honig, R. E. *Surf. Interface Anal.* **1982**, *4*, 35.
(57) Ge, S.; Guo, L.; Rafailovich, M. H.; Sokolov, J.; Peiffer, D. G.; Schwarz, S. A.; Colby, R. H.; Dozier, W. D. *Langmuir* **1999**, *15*, 2911.
(58) Poleunis, C., unpublished results.
(59) Van Krevelen, D. W. *Properties of Polymers-Their Estimation and Correlation with Chemical Structure*, 3rd ed.; Elsevier: New York, 1990; p 198.
(60) Israelachvili, J. N. *Intermolecular and Surface Forces*, 2nd ed.; Academic Press: London, 1992; p 314.
(61) Gutowski, W. In *Fundamentals of Adhesion*; Lee, L.-H., Ed.; Plenum Press: New York, 1991; p 128.
(62) Wu, S. *Polymer Interface and Adhesion*; Marcel Dekker: New York, 1982; p 180.
(63) Fowkes, F. M.; Maruchi, S. *ACS Org. Coat. Plast. Chem. Prepr.* **1977**, *37*, 605.
(64) Georges, E.; Georges, J. M.; Hollinger, S. *Langmuir* **1997**, *13*, 3454.
(65) Iller, R. K. *The Chemistry of Silica*; John Wiley and Sons: New York, 1979; p 645.
(66) Fowkes, F. M. *Ind. Eng. Chem.* **1964**, *56*, 40.

MA990364F